Journal of Computational Applied Mechanics 2022, 53 (3): 393-413

DOI: 10.22059/jcamech.2022.345384.736

RESEARCH PAPER

Buckling analysis of 2D functionally graded porous beams using novel higher order theory

Chandra Mohan Reddy *, Venu Kumar Nathi

Mechanical Engineering, School of Technology, GITAM, Hyderabad, 502329, India

Abstract

Functionally graded material is an in-homogeneous composite, constructed from various phases of material elements, often ceramic and metal and is employed in high-temperature applications. Aim of this work is to examine the behaviour of buckling in porous Functionally Graded Material Beams (FGBs) in 2 directions (2D) with help of fifth order shear deformation theory.
With help of potential energy principle and Reddy's beam theory, equilibrium equations for linear buckling were derived. Boundary conditions such as simply supported – Simply supported (SS), Clamped – clamped (CC) and Clamped-Free (CF) were employed. A unique shear shape function was derived and 5th order theory was adapted to take into account the effect of transverse shear deformation to get the zero shear stress conditions at top and bottom surfaces of the beam. Based on power law, FGB material properties were changed in length and thickness directions. The displacement functions in axial directions were articulated in algebraic polynomials, including admissible functions which were used to fulfil different boundary conditions. Convergence and verification were performed on computed results with results of previous studies. It was found that the results obtained using 5th order theory were in agreement and allows for better buckling analysis for porous material.

Keywords: Buckling Behaviour; Fifth Order Shear Deformation Theory; Lagrange's equations;2D FGB.

1. Introduction

Functionally graded material (FGM) [1] was first introduced in Japan in the mid1980s, for applications in various structural and functional requirements due to necessity of materials capable of resisting high temperature as well as of high strength. FGM belongs to an advanced class of composite materials and characterized [2] by continuous variation of properties as the dimension varies. A typical FGM is an in-homogeneous composite, constructed from various phases of material elements, often ceramic and metal, and is employed in high-temperature applications [3]. In FGM, the mixing of metal and ceramic with acceptable volume fractions offers smooth and continuous fluctuation in mechanical and physical properties in the desired direction. Due to its low thermal conductivity, ceramic component of the material offers resistance to high temperatures. On the other hand, ductile metal component avoids fracture owing to stresses from a high temperature gradient in a relatively short amount of time. And as a result, the FGM structural components can benefit from the advantages of both metals and ceramics in low- and high-temperature environments [4, 5].

The main usage of FGM falls in structural applications where the integration of refractoriness and toughness is

*

accomplished. It includes combustion chambers of rocket engines, high performance cutting tools etc. A few examples of applications where FGMs have considerable potential are heat shields for spacecraft, heat exchanger tubes, biomedical implants, flywheels, and plasma facings for fusion reactors. FGM allows for the creation of novel materials for use in chemical plants, nuclear energy reactors, aerospace applications, and other applications that would typically need incompatible materials. In a typical thermal barrier coating for high temperature applications, for instance, a separate layer of ceramic material is bonded to a metallic structure.

A structural part like a beam is frequently subjected to a persistent temperature difference between its end surfaces in high-temperature applications (top and bottom). As a result, the member is subjected to thermal loading due to the facilitation of conductive heat transfer across the beam thickness under steady-state conditions.

There are several beams' theories to describe behaviour of beam type structures. "The oldest and the well-known beam theory is the Euler–Bernoulli beam theory or classical beam theory (CBT). In this theory the free boundary conditions [6, 7] are not satisfied with shear stress on top and bottom surfaces. Shear correction factor (k) id needed to correct the discrepancy in shear force of the first order shear deformation theory. To overcome this drawback, some higher order shear deformation theories have been developed by researchers".

The shear deformation effects are more pronounced in the thick beams than in the slender beams. "These effects are more neglected in the elementary beam theory. In order to describe the correct bending behaviour of thick beams including shear deformation effects and the associated cross-sectional warping, shear deformation theories are required. This can be accomplished by selection of proper kinematics and constitutive models. The function f(x) is included in the displacement field of higher order theory to take into account the effect of transverse shear deformation and to get zero shear stress conditions at top and bottom surfaces of the beam".

Piezoelectric Nano Films (PNFs) are used to create nonlinear continuous model for large amplitude vibration of nano electromechanical resonators under external electric power. "In order to develop differential equations of motion, Hamilton's principle and von Karman's theory were combined by Asemi H. et al. [8]. "For the transverse vibration of double-piezoelectric-nanoplate systems (DPNPS) with initial stress under an external electric voltage, a nonlocal continuum plate model was created". To account for impact of shearing between two piezoelectric nano plates in addition to the typical behaviour of coupling elastic medium, Pasternak foundation model was used by Asemi S. et al. [9]. "Based on nonlocal continuum mechanics, single layer of graphene sheet subjected for post buckling behaviour. According to Von Karman's assumptions, a nonlinear geometrical model was used" by Asemi S. R. et al. [10]. Based on exponential and power law, elastic modulus of beam was varied in thickness direction. Using shear deformation shell theory, free vibration behaviour of a simply supported FGB was determined by Aydogdu et al. [11]. In their study, attention was given to examining the nano beam's dynamic and stability behaviour, affected by the magnetic field, surface energy, and compressive axial stress. For this scenario, it was assumed that the rotating nano beam was under axial compression and was situated in a non-uniform magnetic field. The Gurtin-Murdoch model and the nonlocal elasticity theory were used to take into account the impact of surface energy and interatomic forces on the vibrational behaviour of rotating nano beams Baghani M. et al. [12]. Solutions of static torsion in microtube formed of 2D FGM was presented in their study. The material characteristics were presumptively variable along the microtube's radius and length in accordance with an arbitrary function. With regard to the axial magnetic field's torque effect, the well-known Maxwell's relation was applied. To investigate the impact of small-scale on static torsion of microtube, couple stress theory was used by Barati A. et al. [13]. their paper examined bi-directional functionally graded (FG) nanobeams exposed to a longitudinal magnetic field in terms of transverse vibrations. The small-scale effect was taken into account using the nonlocal elasticity hypothesis by Barati A. et al. [14]. Investigated free vibration behaviour of bi-directional FGPs from refined theory of shear deformation with first order. From Lagrange equations, the equations of motion were obtained by Bathini S. R. [15]. For bending and dynamic behaviour of FG plates, a first-order theory incorporating shear deformation was developed. The governing equations of axial and transverse deformations of FGPs were developed using 1st order plate theory with shear deformation by Bellifa H. et al. [16]. their study examined the small-scale effects on the functionally graded nanoplate's free vibration behaviour. The small-scale effects on natural frequencies were investigated using the Eringen's nonlocal hypothesis. While stocky and short nanoplates were taken into account, higher order shear deformation plate theory was adapted in order to provide more precise results when analysing the nanoplate by Daneshmehr A. et al. [17]. Based on 3rd order beam theory with shear deformation, free vibration characteristics of FG nano beams were investigated by presenting a Navier type solution. Along thickness direction, the material properties of FG nano beam were changed continuously as per power-law by Ebrahimi et al. [18]. "In their study, attention was given to examine nano beam's dynamic and stability in a generic condition of non-uniform bending stress. Higher order deformation theory was used to develop the governing equations of motion for a functionally graded material plate" by Hadji et al. [19]. Various higher order shear deformation theories have been established for bending and free vibration of FG plates. The pull-in behaviour of functionally graded materials (FGM) cantilever micro/nano-beams under the influence of electrostatic force was studied. By adopting the skew-symmetric portion of the rotation gradients, the coupling tensor becomes skew-symmetric fulfilling consistent couple stress theory by Haghshenas Gorgani H. et al. [20]. 2D and quisi 3D theories of shear deformation were used to analyze behaviour of free vibration, static bending and elastic buckling of FGB with simply supported by Hebbar N. et al. [21]. Based on the notion of strain gradients, the stress distribution in a functionally graded nanodisk of varying thickness was examined. When a nanodisk rotates at a constant angular velocity, it is presumed to be under thermal and mechanical loads Hosseini, M. et al. [22]. To study composite nanoplate's nonlinear vibration analysis lipid face sheets and a functional graded (FG) core were used to create a composite nanoplate. The FG core's material characteristics vary in three different directions. The viscoelastic impact of the lipid layers was investigated using the Kelvin-Voigt model. The nonlinear differential equation of the vibration analysis of the composite nanoplate was obtained utilising the Von-Karman hypotheses by Huang Y. et al. [23]. "Using higher order theory of shear and normal deformation, free vibration analysis of FG elastic, rectangular, and simply supported plates was described. Although heterogeneous, the mechanical characteristics of FG material were modified smoothly with regard to spatial coordinates" by Jha et al. [24]. Two directional FG beams behaviour of buckling was presented with various boundary conditions. Properties of beam material were changed by accommodating various gradation exponents in x and z directions by Karamanlı [25]. Based on Winkler and Pasternak elastic foundation, the free vibration of homogeneous and FG plates was testing. The elastic foundation was a combination of Pasternak and Winkler electric support with parabolically and linearly variable stiffness coefficients along the directions by Ketabdari M. J. et al. [26]. Bidirectional functionally graded nanobeams' ability to bend under magnetic and mechanical force was examined. It was assumed that the Winkler-Pasternak foundation supports the nanobeam. The mechanical behaviour of nanobeam was described using Eringen's nonlocal elasticity theory and the Timoshenko beam model by Khoram et al. [27]. By using classical and first order shear deformation plate theories, the bending, free vibration, and buckling responses of FG porous micro-plates were investigated by Kim et al. [28]. Presented bending and analysis of free vibration of FGB on natural surface position of shear deformation theory. Boundary settings were satisfied with no shear correction factor by Larbi et al. [29]. The free vibration behaviour of a rectangular graphene sheet subjected to a shear in-plane force was investigated. "The vibration analysis of orthotropic single-layered graphene sheets (SLGSs) exposed to shear in-plane force has been studied using nonlocal elasticity theory" by Mohammadi M. et al. [30]. Lipid face sheets and a functional graded (FG) core are used to create a composite nanoplate to study the composite nanoplate's nonlinear vibration analysis. The FG core's material characteristics vary in three different directions. The viscoelastic impact of the lipid layers was investigated using the Kelvin-Voigt model. "The nonlinear differential equation of the vibration analysis of the composite nanoplate was obtained utilising the Von-Karman hypotheses" by Mohammadi M. et al. [31]. In their investigation of vibration analysis, the FG material with core and two layers of lipid were used. The nonlinear differential governing equations were derived from nonlocal elasticity theory. The viscoelastic action of the lipid layers were modelled using the Kelvin-Voigt equation by Mohammadi M. et al. [31, 32]. The small-scale consequences of buckling in a nanoplate constructed from any arbitrary bi-directional functionally graded (BDFG) materials were examined. The effects on buckling load at tiny scales were investigated using the Eringen's nonlocal theory. The least potential energy method was used to obtain the governing equations by Nejad M. Z. et al. [33]. 1st order beam theory with shear deformation was developed to determine static and vibration of FGBs. Transverse shear stiffness improved by using plane stress and equilibrium equation by Nguyen T.K. et al. [34]. Discussed the effect of size dependency in FG material based on beam theory of Timoshenko. Along the thickness, material properties of FG nano beams were varied based on power law by Rahmani O. et al. [35]. Considered the surface effect in investigation of vibration frequencies of nano beams and for satisfaction of surface balance equations of continuum surface elasticity, to proposed Gurtin-Murdoch model by Safarabadi M. et al. [36]. The fundamental frequency of FGB was investigated using classical, first-order, and third-order theories with various boundary settings by Şimşek M. [37]. Free and forced vibration of a Timoshenko beam with bi-directional functionally graded material was explored under the influence of a moving load. In both axial and thickness dimensions, the beam characteristics varied exponentially by Şimşek M. [38]. Using higher order shear deformation theory, free vibration analysis of a simply supported FG plate with porosity was investigated. The material characteristics of FG porous plate changed over thickness of plate by Slimane, M. et al. [39]. FG material plates were analysed to determine behaviour of vibration and static, based on theory of HSD with modification of transverse displacement by finite element model by Talha M. et al. [40]. FG beams were analysed to determine static bending and vibration analysis with various theories of HSD. With transverse shear strain boundary settings to satisfy top and bottom surface of beam by Thai, H.T et al. [41]. An improved theory of shear deformation was developed for analysis of static bending and vibration of FGBs. The shear correction factor was not necessary by shear deformation theory by Vo, T. P. et al. [42]. Bending and free vibration analysis of FG beams on two-parameter elastic foundations were carried out using simple higher order and normal deformation theory. For this purpose, the shear strain shape function was considered. The proposed theory took into account the effects of transverse shear as well as thickness stretching by Lazreg. H. et al. [19].From the literature, it is observed that most of the studies dealt with analysis on non-porous functionally graded materials such as beams, and plates using first and second order theories. This intrigued us to investigate the effect of porosity in functionally graded materials adapting 5th order theory.

This paper focuses on the critical buckling analysis of 2D-FGBs based on the power-law variation of material properties with various end conditions, aspect ratios, gradient indexes and porosity index. A unique shear shape function was derived and 5th order theory was adapted to take into account the effect of transverse shear deformation to get the zero shear stress conditions at top and bottom surfaces of FG beam.

2. Materials and Methods

In this research work, a rectangular beam of Functionally Graded Material (FGM) with length L in x direction, width b in y direction, and thickness h in z direction is consider as shown in Figure 1. Material properties are assumed to vary continuously along length i.e., x- direction and thickness i.e., z- direction. Through the thickness direction, FGM rectangular beam is created by grading ceramic and metal phases. Here, upper surface (z= +h/2) with metal and lower surface (z= -h/2) with ceramic. The middle surface of beam is the reference surface i.e. (z=0).

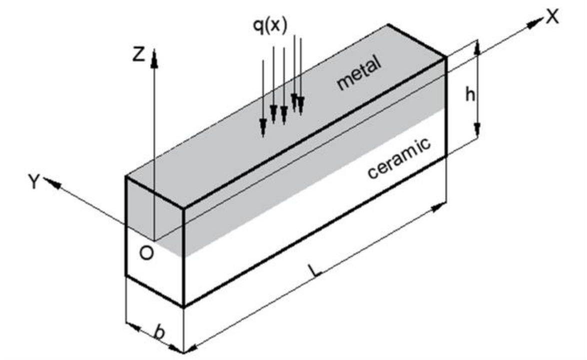

Figure 1: Geometry of Functionally Graded Beam

Material properties of FGBs are the function of volume fraction of constituent materials. The functional relationship between the thickness coordinate and material properties are assumed. The volume fraction of metal (V_m) according to power-law distribution in two directions (x and z) can be expressed as:

$$V_f(x,z) = \left(\frac{z}{h}+\frac{1}{2}\right)^{pz}\left(\frac{x}{L}+\frac{1}{2}\right)^{qx} \tag{1}$$

Where h and z represent the thickness of beam and thickness coordinate, L and x represents the length of beam and length coordinate respectively. Origin (O) is rectangular beam's mid surface (x, y) thus z ϵ [-h/2, h/2]. The Eq.1 shows the relation between volume fraction evolution, thickness and length of beam through power law exponent valves. Here 'p and q' indicates the volume fraction behaviour along beam's thickness and length Figure 2 shows variation of volume fractions of metal in thickness and length direction.

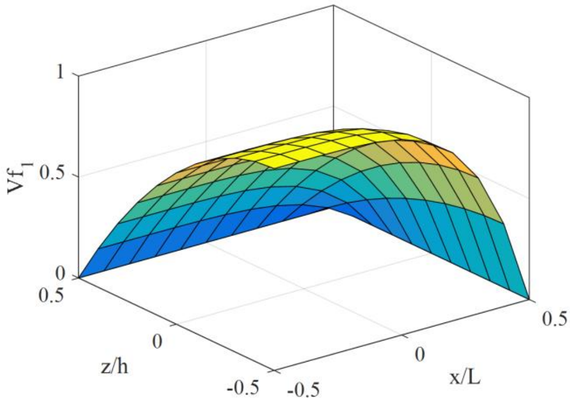

Figure 2: Volume fractions of metal in thickness (z/h) and length(x/L) direction

2.1 Formulation of Functionally Graded Porous Beams

Porosities appear as a defect in FGBs because of technical and penetration problems in production process. Porosities in the beam are two types namely even and uneven as shown in Figure3. “The properties of efficient material of FG beam such as modulus of elasticity E, Poisson’s ratio γ and mass density ρ, are to be found by using modified rule of mixture in which the porosity represented by α, affects averagely on the material volume fraction of each constituent”. As a result, the material property P(x, z) can be written for each type of porosity in coordinates of x and z directions.

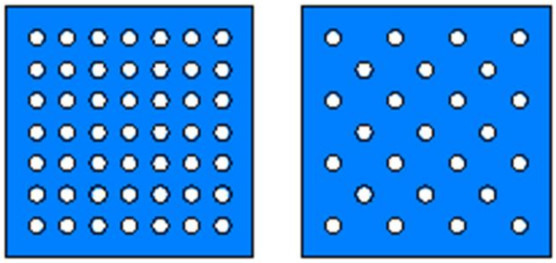

Figure 3: Representation of Bi-Directional FGB with even (a) and uneven (b) porosity distributions

Material properties of functionally graded (FG) material of porous beam (even distribution) can be defined as:

$$P(x,z) = (P_c - P_m)\left(\frac{z}{h}+\frac{1}{2}\right)^{pz}\left(\frac{x}{L}+\frac{1}{2}\right)^{px} + P_m - \frac{\alpha}{2}(P_c + P_m) \tag{2}$$

Here α represents coefficient of porosity which can defined as ratio between void volume and complete volume ($0 \leq \alpha < 1$). “The subscripts m denotes the metal and c denote the ceramic phases. ‘P_x’ and ‘P_z’ are non-negative variables which define the AFG (along axis) and FG (along thickness) power indexes, respectively. These are related to volume fraction change along axis and thickness". The Material properties of beam, i.e. Young’s Modulus ‘E’, Poisson’s ratio ‘v’ and mass density ‘ρ’ of functionally graded material porous beam (even) is given below:

$$E(x,z) = (E_c - E_m)\left(\frac{z}{h}+\frac{1}{2}\right)^{pz}\left(\frac{x}{L}+\frac{1}{2}\right)^{px} + E_m - \frac{\alpha}{2}(E_c + E_m) \tag{3}$$

$$\rho(x,z) = (\rho_c - \rho_m)\left(\frac{z}{h}+\frac{1}{2}\right)^{pz}\left(\frac{x}{L}+\frac{1}{2}\right)^{px} + \rho_m - \frac{\alpha}{2}(\rho_c + \rho_m) \tag{4}$$

The material properties of beam, i.e., Young’s Modulus ‘E’ and mass density ‘ρ’ of functionally graded material porous beam (uneven) is given below:

$$E(x,z) = (E_c - E_m)\left(\frac{z}{h}+\frac{1}{2}\right)^{pz}\left(\frac{x}{L}+\frac{1}{2}\right)^{px} + E_m - \frac{\alpha}{2}(E_c + E_m)\left(1-\frac{2|z}{h}\right) \tag{5}$$

$$\rho(x,z) = (\rho_c - \rho_m)\left(\frac{z}{h}+\frac{1}{2}\right)^{pz}\left(\frac{x}{L}+\frac{1}{2}\right)^{px} + \rho_m - \frac{\alpha}{2}(\rho_c + \rho_m)\left(1-\frac{2|z}{h}\right) \tag{6}$$

2.2 Displacement field and constitutive équations

Consider the functionally graded rectangular beam as shown in (Figure 1), for analytical result of buckling analysis. The accurate buckling of beams depends upon transverse shear and normal deformation. Therefore, any refinement of classical beam theory is generally meaningless. In this regard, the effect of transverse shear and normal strain is considered. The present theory has important features as follows.

The displacement equations are based on Reddy advanced a refined higher order beam theory.

$$U(x,z,t) = u_0(x,t) + z\emptyset(x,t) - f(z)\left(\emptyset(x,t) + \frac{\partial w_0}{\partial x}(x,t)\right) \tag{7}$$

$$W(x,z,t) = w_0(x,t) \tag{8}$$

From above equations, u is axial displacement, w transverse displacements and u_0, w_0 are axial displacement at any point on neutral axis, $\frac{\partial w_0}{\partial x}$ is bending slope and ϕ is shear slope. For determining the distribution of transverse shear deformation, shape function $i.e. f$(z) is used.

$$\varepsilon_x = \frac{\partial U}{\partial x} = \frac{\partial u_0}{\partial x} - z\frac{\partial^2 w_0}{\partial x^2} + f(z)\left(\frac{\partial \phi}{\partial x} + \frac{\partial^2 w_0}{\partial x^2}\right) \tag{9}$$

$$\varepsilon_z = \frac{\partial w}{\partial z} = 0 \tag{10}$$

$$\gamma_{xz} = f'\left[\emptyset + \frac{\partial w_0}{\partial x}\right] \tag{11}$$

$$\boldsymbol{f(z) = \frac{h}{\pi} * sin\left[\frac{\pi * z}{h}\right] - \frac{z}{n*\pi}\left(1 - \frac{1}{n} * \left(\frac{2}{h}\right)^{n-1} * z^{n-1}\right)} \tag{12}$$

$$\boldsymbol{f'(z) = \frac{h}{\pi} * sin\left[\frac{\pi}{h}\right] - \frac{1}{n*\pi}\left(1 - \frac{1}{n} * \left(\frac{2}{h}\right)^{n-1} * (n-1)z^{n-2}\right)} \tag{13}$$

Relationship between stress and strain of two directional FGM beam coordinate axes is given by,

$$\sigma_x = \frac{E(x,z)}{1-\mu^2}\varepsilon_x \tag{14}$$

$$\tau_{xz} = \frac{E(x,z)}{2(1+\mu)}\gamma_{xz} \tag{15}$$

2.3 Formulation of buckling

The strain energy of bi-directional functionally graded beam can be written as:

$$\boldsymbol{U = \frac{1}{2}\int_0^L \int_{-\frac{h}{2}}^{+\frac{h}{2}} (\sigma_x \varepsilon_x + \tau_{xz}\gamma_{xz})\, dz dx} \tag{16}$$

Substituting eq. 9, eq. 11, eq. 14 and eq. 15 into Eq. 16, the strain energy can be obtained and written in the form of:

$$U = \quad \frac{1}{2}\int_0^L \int_{-\frac{h}{2}}^{+\frac{h}{2}} \left(\frac{E(x\, z)}{1-\mu^2}\varepsilon_x \varepsilon_x \; + \frac{E(x\, z)}{2(1+\mu)}\gamma_{xz}\gamma_{xz}\right) dzdx \tag{17}$$

$$U = \frac{1}{2}\int_0^L \int_{-\frac{h}{2}}^{+\frac{h}{2}} \left[\left(\frac{E(x\, z)}{1-\mu^2}\left(\left(\frac{\partial u_0}{\partial x}\right)^2 + \frac{\partial u_0}{\partial x}\frac{d^2 w_0}{dx^2}(2f-2z) + \frac{\partial u_0}{\partial x}\frac{\partial \phi}{\partial x}(2f) + \left(\frac{d^2 w_0}{dx^2}\right)^2 (z^2-2zf+f^2) + \frac{d^2 w_0}{dx^2}\frac{\partial \phi}{\partial x}(2f^2-2zf) + \left(\frac{\partial \phi}{\partial x}\right)^2 (f)^2\right)\right) + \frac{E(x\, z)}{2(1+\mu)}\left(\phi^2 (f')^2 + \phi\frac{\partial w_0}{\partial x}(2f'^2) + \left(\frac{d^2 w_0}{dx^2}\right)^2 (f')^2\right)\right] dzdx \tag{18}$$

From external axial load the potential work can be given by:

$$V = -\frac{1}{2}\int_{-L/2}^{L/2} N_0 \left(\frac{dw}{dx}\right)^2 dx \tag{19}$$

Total potential energy (Π) of the beam is the sum of total strain energy and potential work.

$$\Pi = U + V \tag{20}$$

$$\mathrm{u(x,t)} = \sum_{\mathrm{j=1}}^{\mathrm{m}} \mathrm{A_j \theta_j(x) e^{i\omega t}}, \qquad \theta_j(x) = \left(x+\frac{L}{2}\right)^{p_u}\left(x-\frac{L}{2}\right)^{q_u} x^{m-1} \tag{21}$$

$$w(x,t) = \sum_{j=1}^{m} B_j \varphi_j(x) e^{i\omega t}, \qquad \varphi_j(x) = \left(x+\frac{L}{2}\right)^{p_w}\left(x-\frac{L}{2}\right)^{q_w} x^{m-1} \tag{22}$$

$$\phi(x,t) = \sum_{j=1}^{m} C_j \psi_j(x) e^{i\omega t}, \qquad \psi_j(x) = \left(x+\frac{L}{2}\right)^{p_\phi}\left(x-\frac{L}{2}\right)^{q_\phi} x^{m-1} \tag{23}$$

Boundary conditions proposed $are\;\; \theta_j(x)$,$\varphi_\mathrm{j}(x)$ and $\psi_\mathrm{j}(x)$ as the shape functions and $\boldsymbol{\omega}$ is the natural frequency of beam. To use the complex number $i = \sqrt{-1}$ in determining unknown coefficientsA_j, B_j, and C_j.

By substituting the eq. 21, eq. 22 and eq. 23 in eq. 21 and then by using principle of minimum potential energy eq. 24, the system of equations given in eq. 25 is obtained to calculate critical buckling loads of two directional FGBs.

$$\frac{\partial \Pi}{\partial \mathrm{A_j}} = 0, \frac{\partial \Pi}{\partial \mathrm{B_j}} = 0, \frac{\partial \Pi}{\partial \mathrm{C_j}} = 0 \qquad\qquad \mathrm{j} = 1,2,3, \ldots., \mathrm{m} \tag{24}$$

The values of A_j, B_j and C_j represented with q_j, leads to

$$\left(\begin{bmatrix} [S_{11}] & [S_{12}] & [S_{13}] \\ [S_{12}]^T & [S_{22}] & [S_{23}] \\ [S_{13}]^T & [S_{23}]^T & [S_{33}] \end{bmatrix} - N_{cr}\begin{bmatrix} [0] & [0] & [0] \\ [0] & [K_{\mathrm{N0}}] & [0] \\ [0] & [0] & [0] \end{bmatrix}\right)\begin{Bmatrix} A \\ B \\ C \end{Bmatrix} = \begin{Bmatrix} \{0\} \\ \{0\} \\ \{0\} \end{Bmatrix} \tag{25}$$

The stiffness and geometric stiffness matrices are [Ski] and $[K_{\mathrm{N0}}]$, respectively. The stiffness and geometric stiffness should be symmetric and in max size. The stiffness and geometric stiffness components are given by,

$$S_{11}(i,j) = \int_{-L/2}^{L/2} \frac{E(x,z)}{1-\mu^2}\left[\left(x+\frac{L}{2}\right)^{p\theta}\left(x-\frac{L}{2}\right)^{q\theta} x^{i-1}\left(x+\frac{L}{2}\right)^{p\theta}\left(x-\frac{L}{2}\right)^{q\theta} x^{j-1}\right] dzdx \tag{26}$$

$$S_{12}(i,j) = (f - z)\int_{-L/2}^{L/2} \frac{E(x,z)}{1-\mu^2}\left[\left(x+\frac{L}{2}\right)^{p\theta}\left(x-\frac{L}{2}\right)^{q\theta} x^{i-1}\left(x+\frac{L}{2}\right)^{p\varphi}\left(x-\frac{L}{2}\right)^{q\varphi} x, x^{j-1}\right] dzdx \quad (27)$$

$$S_{13}(i,j) = f\int_{-L/2}^{L/2} \frac{E(x,z)}{1-\mu^2}\left[\left(x+\frac{L}{2}\right)^{p\theta}\left(x-\frac{L}{2}\right)^{q\theta} x^{i-1}\left(x+\frac{L}{2}\right)^{p\psi}\left(x-\frac{L}{2}\right)^{q\psi} x^{j-1}\right] dzdx \quad (28)$$

$$S_{22}(i,j) = (z^2 - zf + f^2)\int_{-\frac{L}{2}}^{\frac{L}{2}} \frac{E(x,z)}{1-\mu^2}\left[\left(x+\frac{L}{2}\right)^{p\varphi}\left(x-\frac{L}{2}\right)^{q\varphi} x, x^{i-1}\left(x+\frac{L}{2}\right)^{p\varphi}\left(x-\frac{L}{2}\right)^{q\varphi} x, x^{j-1}\right] dzdx +$$
$$(f')^2\int_{-\frac{L}{2}}^{\frac{L}{2}} \frac{E(x,z)}{2(1+\mu)}\left[\left(x+\frac{L}{2}\right)^{p\varphi}\left(x-\frac{L}{2}\right)^{q\varphi} x, x^{i-1}\left(x+\frac{L}{2}\right)^{p\varphi}\left(x-\frac{L}{2}\right)^{q\varphi} x, x^{j-1}\right] dzdx \quad (29)$$

$$S_{23}(i,j) = (f^2 - zf)\int_{-\frac{L}{2}}^{\frac{L}{2}} \frac{E(x,z)}{1-\mu^2}\left[\left(x+\frac{L}{2}\right)^{p\varphi}\left(x-\frac{L}{2}\right)^{q\varphi} x, x^{i-1}\left(x+\frac{L}{2}\right)^{p\psi}\left(x-\frac{L}{2}\right)^{q\psi} x^{j-1}\right] dzdx +$$
$$(f')^2\int_{-\frac{L}{2}}^{\frac{L}{2}} \frac{E(x,z)}{2(1+\mu)}\left[\left(x+\frac{L}{2}\right)^{p\varphi}\left(x-\frac{L}{2}\right)^{q\varphi} x^{i-1}\left(x+\frac{L}{2}\right)^{p\psi}\left(x-\frac{L}{2}\right)^{q\psi}\right] dzdx$$
(30)

$$S_{33}(i,j) = (f)^2\int_{-\frac{L}{2}}^{\frac{L}{2}} \frac{E(x,z)}{1-\mu^2}\left[\left(x+\frac{L}{2}\right)^{p\psi}\left(x-\frac{L}{2}\right)^{q\psi} x^{i-1}\left(x+\frac{L}{2}\right)^{p\psi}\left(x-\frac{L}{2}\right)^{q\psi} x^{j-1}\right] + (f')^2\int_{-\frac{L}{2}}^{\frac{L}{2}} \frac{E(x,z)}{2(1+\mu)}\left[\left(x+\frac{L}{2}\right)^{p\psi}\left(x-\frac{L}{2}\right)^{q\psi}\left(x+\frac{L}{2}\right)^{p\psi}\left(x-\frac{L}{2}\right)^{q\psi}\right] dzdx \quad (31)$$

$$K_{N0}(i,j) = \int_{-L/2}^{L/2}\left[\left(x+\frac{L}{2}\right)^{p\varphi}\left(x-\frac{L}{2}\right)^{q\varphi} x, x^{i-1}\left(x+\frac{L}{2}\right)^{p\varphi}\left(x-\frac{L}{2}\right)^{q\varphi} x, x^{j-1}\right] dzdx \quad (32)$$

3. Results

Buckling analysis of 2D FGBs, “which are affected by thickness ratio, aspect ratio, gradation indexes, type of porosity and volume fraction porosity, is presented. The numerical investigations on Simply Supported (SS), Clamped- Clamped (CC) and Clamped-Free (CF) beams at different boundary conditions are carried out” as shown in Table 1.

Table 1: Various kinematic boundary conditions for numerical computations

Boundary condition	X= -L/2	X= L/2
Simply Supported	u=0, w=0	w=0
Clamped-Camped	u=0, w=0, ϕ=0, w’=0	u=0, w=0, ϕ=0, w’=0
Clamped - Free	u=0, w=0, ϕ=0, w’=0	

Buckling behaviour is presented to discuss and validate the accuracy of current theory. Functionally graded material porous beam is considered for numerical results, made of Alumina and Aluminium with the material properties as follows.

Alumina: E_C=380 GPa, $\rho_c = 3960$ kg/m^3, μ_c = 0.3
Aluminium: E_m=70 GPa, $\rho_c = 2702$ kg/m^3, μ_c = 0.3

According to power-law distribution, the functionally graded beam material properties are varying in thickness (h) and axial (L) directions. For representation of results, the following dimensionless critical buckling ($\overline{N}$cr) parameter is used:

$$\overline{N}\mathrm{cr} = \frac{12N_{cr}L^2}{E_2bh^3} \quad (33)$$

Consider the homogeneous beam and different number of terms with displacement functions. The result of dimensionless critical buckling is presented with various gradient indexes in x and z directions, aspect ratios and boundary conditions. For comparison purpose, previous result [19, 25] was used in terms of critical buckling load as shown in Table 2. It can be observed that dimensionless critical buckling of SS, CF and CC beams, the response is very quickly and polynomial expansion is at 6 terms. But for better accuracy purpose, the polynomial expansion at 12 terms was considered. In terms of aspect ratios (L/h=5 and L/h=10) and gradient exponents in both directions (P_x and P_z), dimensionless critical buckling decreases for SS, CC and CF beams while gradient exponents in both directions increased. It is found that the aspect ratio effect becomes very important because the critical buckling increases when the aspect ratio increases, refer in Figure 3, Figure 4 and Figure 5. On other hand, critical buckling value is more in CC beam and critical buckling value is less in CF beam, refer in Table 3, Table4 and Table 5.

It is interesting that the shear deformation effect becomes significantly important as the buckling mode number increases. Critical buckling loads of CC beam with p_x=0 and p_z=0 is 158.9365 and 223.9449 for L/h=5 and L/h=20 respectively. On the other hand, critical buckling loads with P_x=10 and P_z=10 are 29.6924 and 41.4715 respectively. The above differences were obtained while choosing different values of aspect ratio and gradient indexes. The difference is 40% and 25% for the beams whose aspect ratio are L/h=5 and L/h=20. Finally, the reduction in dimensionless critical buckling load because of gradient index variation in x direction is more than gradient index variation in z direction.

Table 2: Verification and convergence studies, dimensionless critical buckling load of FGM beams with respect to various boundary conditions and aspect ratio (L/h) change.

L/h	Theory		Boundary Conditions		
			SS	CC	CF
5	HBT (37)		48.5959	152.1470	13.0594
	RBT (23)		48.5959	152.1474	13.0594
	Present	2 terms	57.9255	158.9365	13.1567
		4 terms	48.6212	154.0366	13.0605
		6 terms	48.5967	152.1476	13.0598
		8 terms	48.5967	152.1476	13.0598
		10 terms	48.5967	152.1476	13.0598
		12 terms	48.5967	152.1476	13.0598
20			53.2364	208.9510	13.3730
			53.2364	208.9514	13.3730
	Present	2 terms	63.1487	223.9449	13.4740
		4 terms	53.2641	212.0982	13.4053
		6 terms	53.2373	208.9520	13.3733
		8 terms	53.2373	208.9520	13.3733
		10 terms	53.2373	208.9520	13.3733
		12 terms	53.2373	208.9520	13.3733

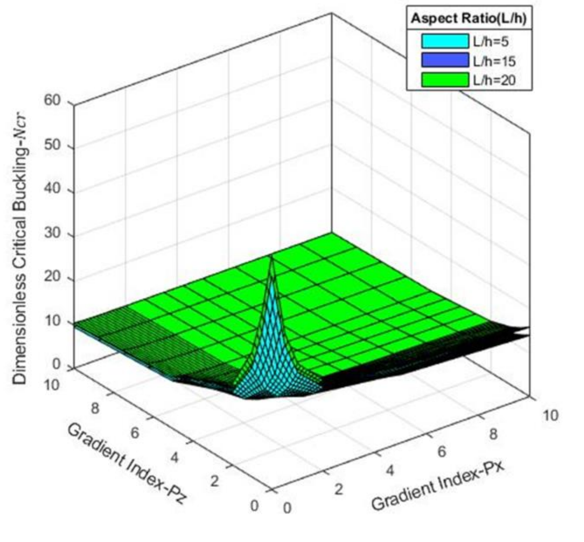

Figure 4: Changes in Dimensionless Critical Buckling(Ncr) of SS beam at various aspect ratios and gradient index along x- direction and z-direction.

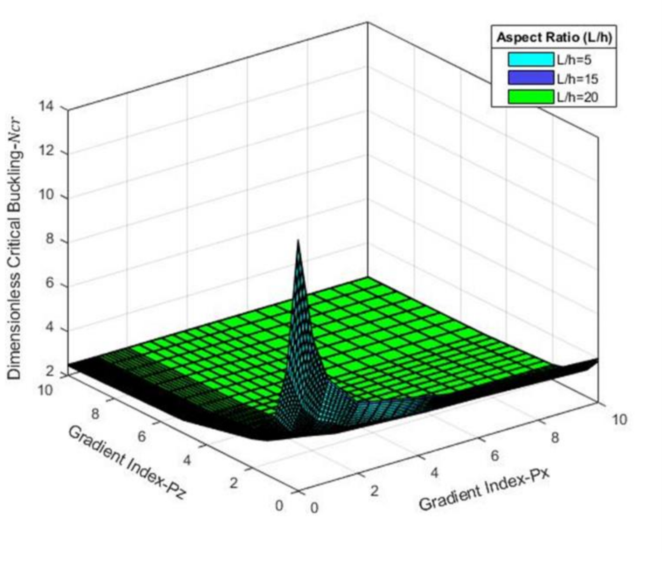

Figure 5: Changes in Dimensionless Critical Buckling (Ncr) of CF beam at various aspect ratios and gradient index along x-direction and z-direction.

Table 3: Influence of gradient exponents and aspect ratio on Dimensionless Critical Buckling (Ncr) of a simply Supported (SS) bi-directional FGB, L/h=5 and L/h=20.

Beam Theory		Px	L/h=5 Pz 0	0.5	1	2	5	10	L/h=20 Pz 0	0.5	1	2	5	10
PRESENT	2 terms	0	57.9255	39.9844	34.1754	27.7932	20.6974	16.8085	63.1487	44.1455	39.1361	32.1206	26.0992	19.0721
	4 terms		48.6212	32.1832	24.8970	19.1813	15.9522	14.0891	53.2641	34.7554	26.5762	20.8298	17.5939	16.2188
	6 terms		48.5967	31.8671	24.5846	19.0717	15.6443	14.052	53.2373	34.538	26.5628	20.7194	17.4851	15.9108
	8terms		48.5967	31.8671	24.5846	19.0717	15.6443	14.052	53.2373	34.538	26.5628	20.7194	17.4851	15.9108
	10terms		48.5967	31.8671	24.5846	19.0717	15.6443	14.052	53.2373	34.538	26.5628	20.7194	17.4851	15.9108
	12terms		48.5967	31.8671	24.5846	19.0717	15.6443	14.052	53.2373	34.538	26.5628	20.7194	17.4851	15.9108
PRESENT	2 terms	0.5	42.1948	32.9583	26.3422	22.1370	17.4962	14.9984	46.0124	34.1355	29.2454	24.7136	19.8606	16.2300
	4 terms		36.2622	24.2707	21.6925	18.0601	14.2708	13.2486	40.8332	28.8303	22.8219	18.8080	16.7887	15.7644
	6 terms		34.2661	23.9975	19.5814	16.2418	13.9975	12.7551	38.5498	26.5212	21.5104	17.8789	15.6763	14.3517
	8terms		34.2661	23.9975	19.5814	16.2418	13.9975	12.7551	38.5498	26.5212	21.5104	17.8789	15.6763	14.3517
	10terms		34.2661	23.9975	19.5814	16.2418	13.9975	12.7551	38.5498	26.5212	21.5104	17.8789	15.6763	14.3517
	12terms		34.2661	23.9975	19.5814	16.2418	13.9975	12.7551	38.5498	26.5212	21.5104	17.8789	15.6763	14.3517
PRESENT	2 terms	1	34.3150	29.9112	22.4256	19.2858	15.8368	13.9927	37.4197	33.2965	24.0944	20.7095	17.1008	15.1566
	4 terms		26.7018	20.0436	18.3474	16.0315	13.5911	11.9714	30.8095	23.8067	20.7983	16.7845	15.7654	14.7412
	6 terms		24.9841	18.9438	16.3134	14.2739	12.7432	11.777	28.5114	21.1158	18.0351	15.7654	14.2178	13.1639
	8terms		24.9841	18.9438	16.3134	14.2739	12.7432	11.777	28.5114	21.1158	18.0351	15.7654	14.2178	13.1639
	10terms		24.9841	18.9438	16.3134	14.2739	12.7432	11.777	28.5114	21.1158	18.0351	15.7654	14.2178	13.1639
	12terms		24.9841	18.9438	16.3134	14.2739	12.7432	11.777	28.5114	21.1158	18.0351	15.7654	14.2178	13.1639
PRESENT	2 terms	2	26.4353	22.9589	18.5090	16.4247	14.1430	12.9302	28.8270	3.1455	19.9435	17.6957	15.3073	14.0274
	4 terms		17.6782	15.6756	13.6672	12.6546	11.6371	10.6136	20.8377	17.8349	15.8265	14.2125	13.5933	12.7689
	6 terms		16.6305	14.0792	12.9402	12.009	11.172	10.5804	18.6445	15.5444	14.217	13.1936	12.3587	11.7218
	8terms		16.6305	14.0792	12.9402	12.009	11.172	10.5804	18.6445	15.5444	14.217	13.1936	12.3587	11.7218
	10terms		16.6305	14.0792	12.9402	12.009	11.172	10.5804	18.6445	15.5444	14.217	13.1936	12.3587	11.7218
	12terms		16.6305	14.0792	12.9402	12.009	11.172	10.5804	18.6445	15.5444	14.217	13.1936	12.3587	11.7218
PRESENT	2 terms	5	18.5555	16.9583	14.5924	13.5591	12.4353	11.8479	20.2343	17.6524	15.7926	14.6774	13.5000	12.8787
	4 terms		12.6733	11.6707	10.9629	10.6501	10.3323	9.6099	14.1332	13.8303	13.4219	12.3080	11.7887	10.7644
	6 terms		10.9891	10.4125	10.1431	9.8973	9.6208	9.4239	11.9315	11.281	10.9963	10.7647	10.5351	10.3466
	8terms		10.9891	10.4125	10.1431	9.8973	9.6208	9.4239	11.9315	11.281	10.9963	10.7647	10.5351	10.3466
	10terms		10.9891	10.4125	10.1431	9.8973	9.6208	9.4239	11.9315	11.281	10.9963	10.7647	10.5351	10.3466
	12terms		10.9891	10.4125	10.1431	9.8973	9.6208	9.4239	11.9315	11.281	10.9963	10.7647	10.5351	10.3466
PRESENT	2 terms	10	14.9738	12.9112	12.8121	12.2538	11.6539	11.3460	17.3286	15.0847	13.9058	13.3028	12.6734	12.3468
	4 terms		10.6463	10.2436	9.8357	9.6225	9.4036	9.1808	12.8095	12.2067	11.7983	11.3845	10.7654	10.2412
	6 terms		9.5846	9.423	9.3411	9.2555	9.1472	9.079	10.351	10.1871	10.1164	10.0577	9.9951	9.9442
	8terms		9.5846	9.423	9.3411	9.2555	9.1472	9.079	10.351	10.1871	10.1164	10.0577	9.9951	9.9442
	10terms		9.5846	9.423	9.3411	9.2555	9.1472	9.079	10.351	10.1871	10.1164	10.0577	9.9951	9.9442
	12terms		9.5846	9.423	9.3411	9.2555	9.1472	9.079	10.351	10.1871	10.1164	10.0577	9.9951	9.9442

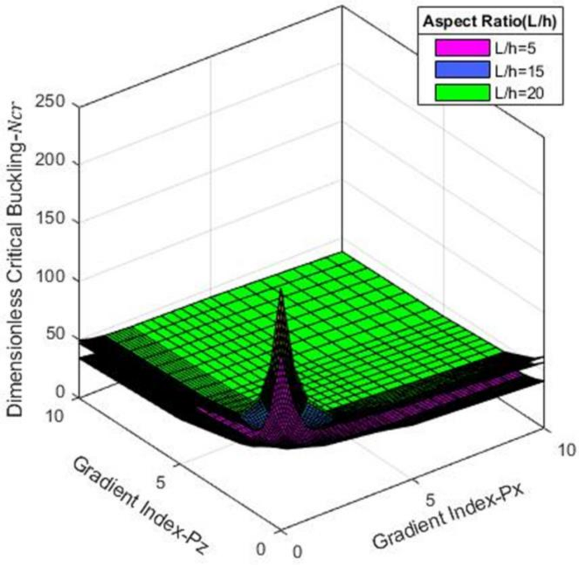

Figure 6: Changes in Dimensionless Critical Buckling(Ncr) of CC beam at various aspect ratios and gradient index along x- direction and z-direction.

Table 4: Influence of gradient exponents and aspect ratio on Dimensionless Critical Buckling (Ncr) of a Clamped–Free (CF) bi-directional FGB, L/h=5 and L/h=20.

		Px	L/h=5		Pz				L/h=20		Pz			
Beam Theory			0	0.5	1	2	5	10	0	0.5	1	2	5	10
PRESENT	2 terms	0	13.1567	8.5002	6.5813	6.1569	4.2806	4.0025	13.474	9.4362	7.4292	6.3097	4.4942	4.1011
	4 terms		13.0605	8.4963	6.5417	6.1269	4.2761	3.9318	13.4053	8.9265	6.828	6.2872	4.4441	4.0458
	6 terms		13.0598	8.4921	6.5355	6.1103	4.2706	3.875	13.3733	8.671	6.6676	6.2429	4.3972	4.0042
	8 terms		13.0598	8.4921	6.5355	6.1103	4.2706	3.875	13.3733	8.671	6.6676	6.2429	4.3972	4.0042
	10 terms		13.0598	8.4921	6.5355	6.1103	4.2706	3.875	13.3733	8.671	6.6676	6.2429	4.3972	4.0042
	12 terms		13.0598	8.4921	6.5355	6.1103	4.2706	3.875	13.3733	8.671	6.6676	6.2429	4.3972	4.0042
PRESENT	2 terms	0.5	8.0567	5.8789	4.9315	4.214	3.5131	3.2319	8.251	6.2037	5.0574	4.3218	3.6011	3.3194
	4 terms		7.2877	5.4698	4.6708	4.0933	3.4932	3.2273	7.4977	5.894	4.7355	4.15	3.5903	3.3184
	6 terms		7.0856	5.245	4.4708	3.8912	3.4851	3.2204	7.1982	5.3258	4.5428	3.9648	3.5756	3.3131
	8terms		7.0856	5.245	4.4708	3.8912	3.4851	3.2204	7.1982	5.3258	4.5428	3.9648	3.5756	3.3131
	10terms		7.0856	5.245	4.4708	3.8912	3.4851	3.2204	7.1982	5.3258	4.5428	3.9648	3.5756	3.3131
	12terms		7.0856	5.245	4.4708	3.8912	3.4851	3.2204	7.1982	5.3258	4.5428	3.9648	3.5756	3.3131
PRESENT	2 terms	1	6.5147	4.0847	4.0071	3.6874	3.189	2.9229	6.6718	4.2582	4.1136	3.7809	3.2682	2.9949
	4 terms		4.9895	3.9618	3.6677	3.4437	3.1156	2.8976	5.2628	4.0385	3.8344	3.5326	3.1676	2.9713
	6 terms		4.7501	3.9273	3.5693	3.288	3.0559	2.8895	4.8131	3.981	3.6224	3.3467	3.1293	2.966
	8terms		4.7501	3.9273	3.5693	3.288	3.0559	2.8895	4.8131	3.981	3.6224	3.3467	3.1293	2.966
	10terms		4.7501	3.9273	3.5693	3.288	3.0559	2.8895	4.8131	3.981	3.6224	3.3467	3.1293	2.966
	12terms		4.7501	3.9273	3.5693	3.288	3.0559	2.8895	4.8131	3.981	3.6224	3.3467	3.1293	2.966
PRE	2 terms	2	5.5069	3.984	3.7308	3.3403	2.9715	2.7775	5.6397	4.212	3.8246	3.4242	3.0449	2.8456
	4 terms		3.8641	3.4642	3.3333	3.1535	2.7731	2.6319	4.013	3.512	3.409	3.2565	2.7931	2.7231

SENT	6 terms		3.3266	3.0399	2.9109	2.8034	2.6995	2.6201	3.3687	3.0812	2.9544	2.8531	2.7605	2.6848
	8terms		3.3266	3.0399	2.9109	2.8034	2.6995	2.6201	3.3687	3.0812	2.9544	2.8531	2.7605	2.6848
	10terms		3.3266	3.0399	2.9109	2.8034	2.6995	2.6201	3.3687	3.0812	2.9544	2.8531	2.7605	2.6848
	12terms		3.3266	3.0399	2.9109	2.8034	2.6995	2.6201	3.3687	3.0812	2.9544	2.8531	2.7605	2.6848
PRESENT	2 terms	5	4.562	3.4789	3.3246	3.0562	2.8038	2.672	4.672	3.6037	3.4075	3.1323	2.8727	2.7373
	4 terms		3.3575	2.8698	2.7002	2.6876	2.6751	2.5687	3.8074	2.9172	2.7652	2.7209	2.6963	2.6221
	6 terms		2.6056	2.549	2.5225	2.4985	2.4713	2.4517	2.6448	2.59	2.5661	2.5466	2.5266	2.5099
	8terms		2.6056	2.549	2.5225	2.4985	2.4713	2.4517	2.6448	2.59	2.5661	2.5466	2.5266	2.5099
	10terms		2.6056	2.549	2.5225	2.4985	2.4713	2.4517	2.6448	2.59	2.5661	2.5466	2.5266	2.5099
	12terms		2.6056	2.549	2.5225	2.4985	2.4713	2.4517	2.6448	2.59	2.5661	2.5466	2.5266	2.5099
PRESENT	2 terms	10	3.8716	3.1407	3.0402	2.8602	2.6912	2.6032	3.965	3.2582	3.1153	2.9307	2.757	2.6666
	4 terms		3.2895	2.8218	2.6736	2.6679	2.5623	2.4594	3.4632	2.892	2.7761	2.7151	2.5859	2.5097
	6 terms		2.4602	2.4458	2.4387	2.4312	2.422	2.4161	2.5042	2.4917	2.4865	2.482	2.4773	2.4734
	8terms		2.4602	2.4458	2.4387	2.4312	2.422	2.4161	2.5042	2.4917	2.4865	2.482	2.4773	2.4734
	10terms		2.4602	2.4458	2.4387	2.4312	2.422	2.4161	2.5042	2.4917	2.4865	2.482	2.4773	2.4734
	12terms		2.4602	2.4458	2.4387	2.4312	2.422	2.4161	2.5042	2.4917	2.4865	2.482	2.4773	2.4734

Table 5: Influence of gradient exponents and aspect ratio on Dimensionless Critical Buckling (Ncr) of a Clamped –Clamped (CC) bi-directional FGB, L/h=5 and L/h=20

Beam Theory		Px	L/h=5			Pz			L/h=20			Pz		
			0	0.5	1	2	5	10	0	0.5	1	2	5	10
PR	2 terms	0	158.9365	122.5485	99.6567	75.3119	61.868	55.6679	223.9449	145.3673	120.7954	92.0269	75.6084	68.0466
E	4 terms		154.0366	109.2299	88.7769	67.1795	55.1166	49.5197	212.0982	136.3455	111.601	84.3995	69.26	62.2636
S	6 terms		152.1476	102.2706	79.4841	60.8789	46.8876	40.989	208.952	135.87	104.564	81.4659	68.3278	61.9983
E	8 terms		152.1476	102.2706	79.4841	60.8789	46.8876	40.989	208.952	135.87	104.564	81.4659	68.3278	61.9983
N	10 terms		152.1476	102.2706	79.4841	60.8789	46.8876	40.989	208.952	135.87	104.564	81.4659	68.3278	61.9983
T	12 terms		152.1476	102.2706	79.4841	60.8789	46.8876	40.989	208.952	135.87	104.564	81.4659	68.3278	61.9983
R	2 terms	0.5	127.8892	93.2582	75.2935	62.3699	54.1302	49.3828	151.5329	115.2725	92.0089	76.2192	66.1587	60.3617
E	4 terms		106.0476	81.2347	66.8361	55.4874	48.2014	44.0127	141.7227	107.3517	84.0137	69.7473	60.6042	55.3477
S	6 terms		99.2477	72.5799	60.1899	49.6849	41.0621	37.0583	137.997	97.6901	80.4927	67.6312	59.417	54.6238
E	8terms		99.2477	72.5799	60.1899	49.6849	41.0621	37.0583	137.997	97.6901	80.4927	67.6312	59.417	54.6238
N	10terms		99.2477	72.5799	60.1899	49.6849	41.0621	37.0583	137.997	97.6901	80.4927	67.6312	59.417	54.6238
T	12terms		99.2477	72.5799	60.1899	49.6849	41.0621	37.0583	137.997	97.6901	80.4927	67.6312	59.417	54.6238
R	2 terms	1	101.4178	81.3095	66.1367	56.972	50.6376	46.7694	122.7763	93.4013	79.5904	68.441	60.4662	56.6593
E	4 terms		78.4186	64.1603	58.8801	50.7441	45.1226	41.6871	113.0688	87.3846	73.9506	63.7547	56.7147	52.4069
S	6 terms		72.0965	57.371	50.0395	43.489	37.7669	34.8965	104.967	79.8061	68.7443	60.2078	54.3487	50.6889
E	8terms		72.0965	57.371	50.0395	43.489	37.7669	34.8965	104.967	79.8061	68.7443	60.2078	54.3487	50.6889
N	10terms		72.0965	57.371	50.0395	43.489	37.7669	34.8965	104.967	79.8061	68.7443	60.2078	54.3487	50.6889
T	12terms		72.0965	57.371	50.0395	43.489	37.7669	34.8965	104.967	79.8061	68.7443	60.2078	54.3487	50.6889
R	2 terms	2	65.339	53.2299	47.4257	42.0262	38.0555	35.7599	83.9394	71.3455	66.5682	57.036	52.4932	45.9645
E	4 terms		52.0859	44.9839	41.2635	37.7752	34.5086	32.7052	77.3668	63.9899	57.8252	52.8705	49.2062	43.0003

S	6 terms		52.0859	44.9839	41.2635	37.7752	34.5086	32.7052	77.3668	63.9899	57.8252	52.8705	49.2062	43.0003
E	8terms		52.0859	44.9839	41.2635	37.7752	34.5086	32.7052	77.3668	63.9899	57.8252	52.8705	49.2062	43.0003
N	10terms		52.0859	44.9839	41.2635	37.7752	34.5086	32.7052	77.3668	63.9899	57.8252	52.8705	49.2062	43.0003
T	12terms		52.0859	44.9839	41.2635	37.7752	34.5086	32.7052	77.3668	63.9899	57.8252	52.8705	49.2062	43.0003
R	2 terms	5	69.572	57.2582	51.7524	47.6821	44.4838	42.3261	71.5203	63.2222	58.2613	54.3607	50.2835	44.726
E	4 terms		51.4789	41.3347	37.9774	34.7934	32.2753	31.6354	64.7068	56.1517	52.1387	49.3398	46.5296	41.0364
S	6 terms		38.8736	35.9539	34.3754	32.8629	31.4291	30.5739	56.6544	51.0849	48.3535	46.064	44.275	39.2438
E	8terms		38.8736	35.9539	34.3754	32.8629	31.4291	30.5739	56.6544	51.0849	48.3535	46.064	44.275	39.2438
N	10terms		38.8736	35.9539	34.3754	32.8629	31.4291	30.5739	56.6544	51.0849	48.3535	46.064	44.275	39.2438
T	12terms		38.8736	35.9539	34.3754	32.8629	31.4291	30.5739	56.6544	51.0849	48.3535	46.064	44.275	39.2438
R	2 terms	10	58.7607	49.1095	46.334	43.9697	41.9739	40.5332	59.4069	54.4013	51.6011	48.3565	45.3177	43.2683
E	4 terms		42.5257	38.2603	35.0544	32.9754	31.2458	30.1158	53.7372	49.5846	47.4422	45.036	43.5163	42.8596
S	6 terms		34.0354	32.4928	31.6666	30.8931	30.1758	29.6924	49.3624	46.2902	44.7404	43.4092	42.3085	41.4715
E	8terms		34.0354	32.4928	31.6666	30.8931	30.1758	29.6924	49.3624	46.2902	44.7404	43.4092	42.3085	41.4715
N	10terms		34.0354	32.4928	31.6666	30.8931	30.1758	29.6924	49.3624	46.2902	44.7404	43.4092	42.3085	41.4715
T	12terms		34.0354	32.4928	31.6666	30.8931	30.1758	29.6924	49.3624	46.2902	44.7404	43.4092	42.3085	41.4715

Table 6: Influence of gradient exponents and porosity distribution on dimensionless critical buckling of a simply supported (SS) bi-directional FGB at aspect ratio L/h=5

	Even Porosity					Uneven Porosity			
Px&Pz	**0**	**0.1**	**0.2**	**0.3**	**Px&Pz**	**0**	**0.1**	**0.2**	**0.3**
0	48.5967	45.7193	42.8418	39.9644	0	48.5967			45.7429
0.5	29.5340	26.9418	24.3844	21.8672	0.5	29.5340	28.6764	27.8117	26.9390
1	20.1681	17.5884	15.0565	12.5794	1	20.1681	19.3115	18.4452	17.5674
2	16.2151	13.5680	10.9572	8.3334	2	16.2151	15.2852	14.3322	13.3492
5	12.7122	9.9435	7.1980	4.0961	5	12.7122	11.7151	10.6875	9.6199
10	10.9131	8.0461	5.1912	2.2872	10	10.9131	9.8839	8.8196	7.7124

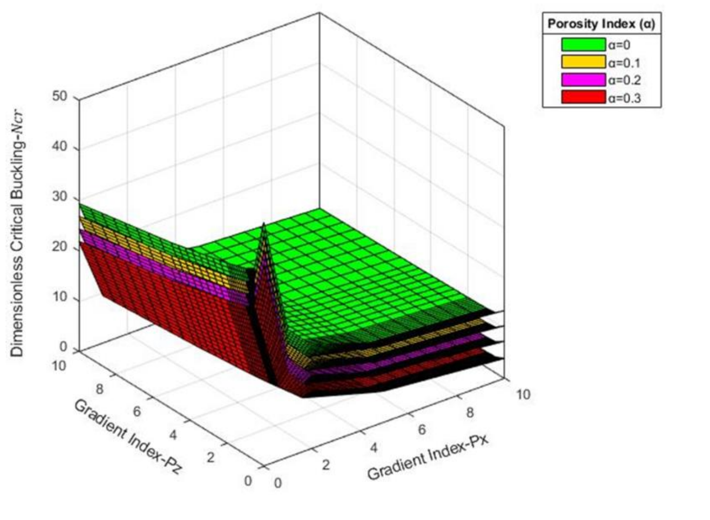

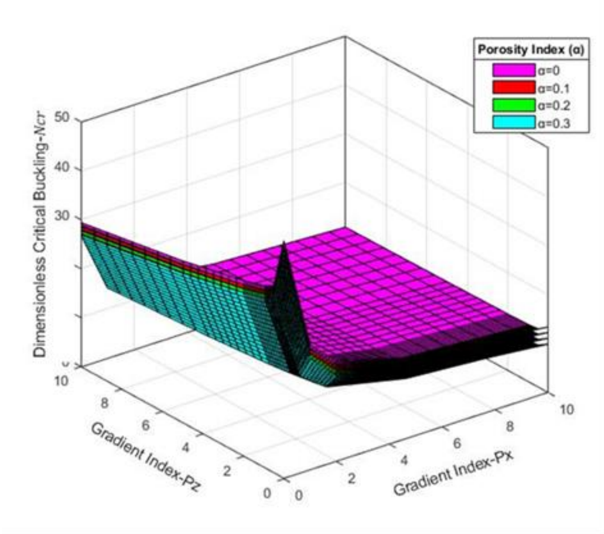

Figure 7: Dimensionless critical buckling of SS beam with even porosity(a) and uneven porosity(b) at aspect ratio L/h=5

Table 7: Influence of gradient exponents and porosity distribution on dimensionless natural frequencies of a clamped free (CF) bi-directional FGB at aspect ratio L/h=5

	Even Porosity					Uneven Porosity			
Px&Pz	**0**	**0.1**	**0.2**	**0.3**	**Px&Pz**	**0**	**0.1**	**0.2**	**0.3**
0	13.0598	12.2865	11.5133	10.73998	0	13.0598	12.8188	12.5774	12.3354
0.5	5.2450	4.9344	4.6239	4.3133	0.2	5.2450	5.1482	5.0513	4.9541
1	3.5693	3.1392	2.7091	2.2790	0.4	3.5693	3.4347	3.2995	3.1636
2	2.8034	2.5895	1.9729	1.5466	0.6	2.8034	2.6656	2.5254	2.3820
5	2.4713	2.4097	1.8442	1.1850	0.8	2.4713	2.4314	2.4010	2.3705
10	2.4161	2.2491	1.5878	0.8744	1	2.4161	2.2919	2.1773	2.1180

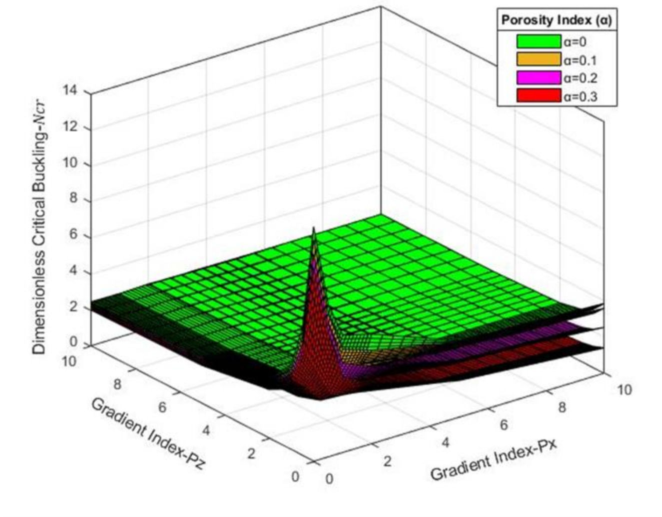

(a)

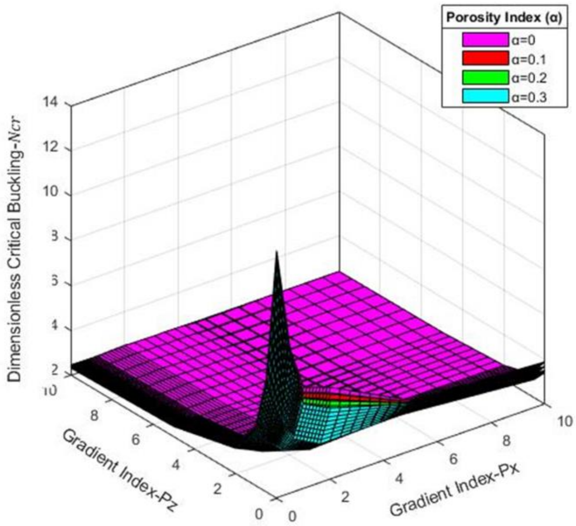

(b)

Figure8: Dimensionless critical buckling of CF beam with even porosity(a) and uneven porosity(b) at aspect ratio L/h=5

Table 8: Influence of gradient exponents and porosity distribution on dimensionless natural frequencies of a clamped –clamped (CC) bi-directional FGB at aspect ratio L/h=5

Px&Pz	Even Porosity				Px&Pz	Uneven Porosity			
	0	0.1	0.2	0.3		0	0.1	0.2	0.3
0	152.1476	143.1385	134.1298	125.1211	0	152.1476	149.4467	146.7450	144.0420
0.5	79.5799	66.9392	56.0951	43.8802	0.5	79.5799	74.0703	70.8625	67.5864
1	50.0395	40.5802	29.6512	16.2285	1	50.0395	47.6853	44.4575	41.1400
2	37.7752	30.5594	19.9019	8.0306	2	37.7752	37.5312	34.3137	30.9742
5	31.4291	24.3759	14.3698	3.4870	5	31.4291	31.0705	28.0959	25.0209
10	29.6924	21.4129	12.0228	2.1304	10	29.6924	27.8827	25.1091	22.2949

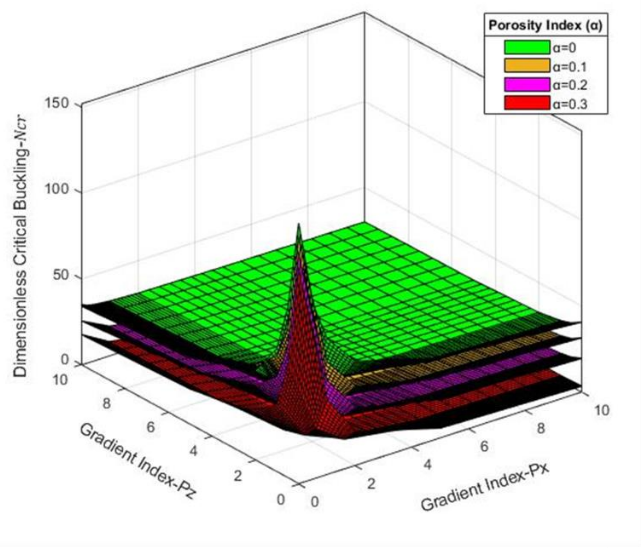

(a)

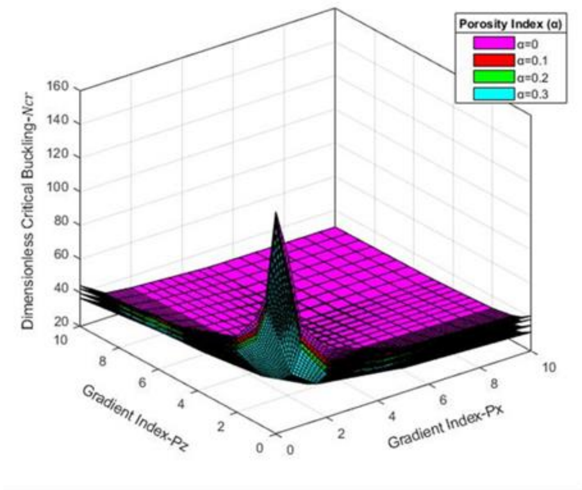

(b)

Fig 9. Dimensionless critical buckling of CF beam with even porosity(a) and uneven porosity(b) at aspect ratio L/h=5

4. Discussion

Figure 7 shows the dimensionless critical buckling load versus the gradient indexes in length (p_x) and thickness (p_z) direction for different porosity distribution patterns when α = 0.1. It can be observed that the difference between different porosity distribution patterns can be reduced with increase in gradient index. "Which indicates that the porosity distribution in the thickness (z) direction has greater influence on critical buckling than the axial porosity (x direction) distribution."

Figure. 8and Figure. 9 illustrate the dimensionless critical buckling load versus gradient indexes in length (p_x)and thickness (p_z) direction **of** beam and the total volume fraction of porosity in different modes, respectively. It can be seen that the sensitivity of critical buckling to the gradient index of beam and total volume fraction of porosity is improved with increase of buckling mode number.

Table 6. Showscritical buckling of SS beam that decreases with increase in porosity index, and decreases with increase in gradation exponents in x and z directions. Critical buckling value is more in uneven porosity distribution when compared with even porosity distribution.

Table 7 showscritical buckling of CF beam decreases with increase in porosity index, and decreases with increase in gradation exponents in x and z directions. Critical buckling value is more in uneven porosity distribution when compared with even porosity distribution. Table 8. Showscritical buckling value of CC beam decreases with increase in porosity index, and decreases with increase in gradation exponents in x and z directions. Critical buckling value is more in uneven porosity distribution when compared with even porosity distribution.

5. Conclusion

Two directional FG porous beams were analysed for behaviour of buckling, subjected to various boundary conditions (SS, CS, CC, and CF) with UDL. Considering these boundary conditions with different aspect ratios and gradation exponents in x and z directions. 5^{th} order shear deformation theory was adapted to determine free critical buckling with even and uneven porosity distribution. Based on power-law distribution, effective properties of FG porous beams in two directions were determined. The effect of boundary conditions, distribution of porosity, aspect ratios, and gradation exponents on critical buckling analysis through several numerical illustrations was highlighted.

The computed results are compared to those from earlier investigations in terms of dimensionless critical buckling loads. The calculated outcomes are found to have a very good correlation with earlier ones. Aspect ratios, gradient indexes, and boundary conditions' impacts on the 2D-FGBs' critical buckling loads was explored. The most significant findings w.r.t non porous FGBs are listed below:

- The gradient indexes have a significant impact on the dimensionless critical buckling loads of the 2D-FGBs. However, the gradient index's impact in the x direction is more profound than its impact in the z direction.
- As the buckling mode number increases, the shear deformation effect becomes more significant. For all varieties of BCs, as the buckling mode increases, so does the relative difference between the critical buckling loads.

- The shear deformation effect on the critical buckling loads of the 2D-FGBs reduces as the aspect ratio increases. The CC 2D-FGB is found to be significantly more susceptible to the shear deformation effect than the other 2D-FGB models.

- CC beams experience the highest first critical buckling stresses, followed by SS and CF beams.

- By choosing the appropriate gradient indexes, the vibration and buckling behaviours of the 2D-FGBs may be regulated to match the design requirements.

- The shear deformation impact is quite significant, especially for thick beams, and the proposed theory yields accurate findings and is effective in resolving the vibration and buckling behaviours of the 2D-FGBs.

The suggested two-directionally porous beam model is used to examine the buckling behaviour of two-directionally porous beams. The most significant findings w.r.t porous FGBs are listed below:

- When the volume percentage of porosity increases close to the middle surface, the critical buckling load will increase for the same total volume fraction of porosity.

- The effect of porosity distribution in the thickness direction is more dominant than the effect of axial direction on the critical buckling load.

The porosity parameter is a crucial parameter that must be considered in design of modern structures and the percentage of porosity in structure can be affected considerably in its performance and response. The proposed method shall be useful to analyse the shear deformation of FGBs, where these FGB surfaces are subjected to high temperature at one end and low temperature at the other end.

Nomenclature

x, y, z	Different coordinates along length, width, thickness directions of beam
2D	Two dimensional
FGB	Functionally graded beam
SS	Simply supported
CC	Clamped-clamped
CF	Clamped free
FGM	Functionally graded material
L	length
h	height
V_f	Volume fraction
P_z	Gradient index in thickness direction
q_x	Gradient index in length direction
CBT	Classical beam theory
K	Shear correction factor
F(z)	Shear shape function
FG	Functionally graded
DPNPS	double-piezoelectric-nanoplate systems
SLGS	single-layered graphene sheets
HSDT	higher order shear deformation plate theory
3D	Three dimensional
FGP	Functionally graded plate
HSD	Higher order deformation
E	modulus of elasticity
μ	Poisson's ratio
ρ	mass density
α	coefficient of porosity
f(z)	Shear shape function
σ_x	Axial stress
τ_{xz}	Shear stress

Π	potential energy
U	Strain energy
V	potential work

References

[1] M. Hosseini, M. Shishesaz, K. N. Tahan, A. Hadi, Stress analysis of rotating nano-disks of variable thickness made of functionally graded materials, *International Journal of Engineering Science,* Vol. 109, pp. 29-53, 2016.

[2] M. Mohammadi, M. Safarabadi, A. Rastgoo, A. Farajpour, Hygro-mechanical vibration analysis of a rotating viscoelastic nanobeam embedded in a visco-Pasternak elastic medium and in a nonlinear thermal environment, *Acta Mechanica,* Vol. 227, No. 8, pp. 2207-2232, 2016.

[3] M. Mohammadi, A. Farajpour, M. Goodarzi, R. Heydarshenas, Levy Type Solution for Nonlocal Thermo-Mechanical Vibration of Orthotropic Mono-Layer Graphene Sheet Embedded in an Elastic Medium, *Journal of Solid Mechanics,* Vol. 5, No. 2, pp. 116-132, 2013.

[4] A. Farajpour, A. Rastgoo, M. Mohammadi, Surface effects on the mechanical characteristics of microtubule networks in living cells, *Mechanics Research Communications,* Vol. 57, pp. 18-26, 2014/04/01/, 2014.

[5] M. Mohammadi, A. Farajpour, A. Moradi, M. Hosseini, Vibration analysis of the rotating multilayer piezoelectric Timoshenko nanobeam, *Engineering Analysis with Boundary Elements,* Vol. 145, pp. 117-131, 2022/12/01/, 2022.

[6] M. Mohammadi, M. Ghayour, A. Farajpour, Free transverse vibration analysis of circular and annular graphene sheets with various boundary conditions using the nonlocal continuum plate model, *Composites Part B: Engineering,* Vol. 45, No. 1, pp. 32-42, 2013.

[7] M. Mohammadi, M. Hosseini, M. Shishesaz, A. Hadi, A. Rastgoo, Primary and secondary resonance analysis of porous functionally graded nanobeam resting on a nonlinear foundation subjected to mechanical and electrical loads, *European Journal of Mechanics - A/Solids,* Vol. 77, pp. 103793, 2019/09/01/, 2019.

[8] H. Asemi, S. Asemi, A. Farajpour, M. Mohammadi, Nanoscale mass detection based on vibrating piezoelectric ultrathin films under thermo-electro-mechanical loads, *Physica E: Low-dimensional Systems and Nanostructures,* Vol. 68, pp. 112-122, 2015.

[9] S. R. Asemi, A. Farajpour, H. R. Asemi, M. Mohammadi, Influence of initial stress on the vibration of double-piezoelectric-nanoplate systems with various boundary conditions using DQM, *Physica E: Low-dimensional Systems and Nanostructures,* Vol. 63, pp. 169-179, 2014.

[10] S. R. Asemi, M. Mohammadi, A. Farajpour, A study on the nonlinear stability of orthotropic single-layered graphene sheet based on nonlocal elasticity theory, *Latin American Journal of Solids and Structures,* Vol. 11, No. 9, pp. 1515-1540, 2014.

[11] M. Aydogdu, V. Taskin, Free vibration analysis of functionally graded beams with simply supported edges, *Materials & design,* Vol. 28, No. 5, pp. 1651-1656, 2007.

[12] M. Baghani, M. Mohammadi, A. Farajpour, Dynamic and Stability Analysis of the Rotating Nanobeam in a Nonuniform Magnetic Field Considering the Surface Energy, *International Journal of Applied Mechanics,* Vol. 08, No. 04, pp. 1650048, 2016.

[13] A. Barati, M. M. Adeli, A. Hadi, Static torsion of bi-directional functionally graded microtube based on the couple stress theory under magnetic field, *International Journal of Applied Mechanics,* Vol. 12, No. 02, pp. 2050021, 2020.

[14] A. Barati, A. Hadi, M. Z. Nejad, R. Noroozi, On vibration of bi-directional functionally graded nanobeams under magnetic field, *Mechanics Based Design of Structures and Machines,* Vol. 50, No. 2, pp. 468-485, 2022.

[15] S. R. Bathini, Free vibration behaviour of bi-directional functionally graded plates with porosities using a refined first order shear deformation theory, *Journal of Computational Applied Mechanics,* Vol. 51, No. 2, pp. 374-388, 2020.

[16] H. Bellifa, K. H. Benrahou, L. Hadji, M. S. A. Houari, A. Tounsi, Bending and free vibration analysis of functionally graded plates using a simple shear deformation theory and the concept the neutral surface position, *Journal of the Brazilian Society of Mechanical Sciences and Engineering,* Vol. 38, No. 1, pp. 265-275, 2016.

[17] A. Daneshmehr, A. Rajabpoor, A. Hadi, Size dependent free vibration analysis of nanoplates made of functionally graded materials based on nonlocal elasticity theory with high order theories, *International Journal of Engineering Science,* Vol. 95, pp. 23-35, 2015.

[18] F. Ebrahimi, M. R. Barati, A nonlocal higher-order shear deformation beam theory for vibration analysis of size-dependent functionally graded nanobeams, *Arabian Journal for Science and Engineering,* Vol. 41, No. 5, pp. 1679-1690, 2016.

[19] L. Hadji, F. Bernard, Bending and free vibration analysis of functionally graded beams on elastic foundations with analytical validation, *Advances in materials Research,* Vol. 9, No. 1, pp. 63-98, 2020.

[20] H. Haghshenas Gorgani, M. Mahdavi Adeli, M. Hosseini, Pull-in behaviour of functionally graded micro/nano-beams for MEMS and NEMS switches, *Microsystem Technologies,* Vol. 25, No. 8, pp. 3165-3173, 2019.

[21] N. Hebbar, I. Hebbar, D. Ouinas, M. Bourada, Numerical modeling of bending, buckling, and vibration of functionally graded beams by using a higher-order shear deformation theory, *Frattura ed Integrità Strutturale,* Vol. 14, No. 52, pp. 230-246, 2020.

[22] M. Hosseini, M. Shishesaz, A. Hadi, Thermoelastic analysis of rotating functionally graded micro/nanodisks of variable thickness, *Thin-Walled Structures,* Vol. 134, pp. 508-523, 2019.

[23] Y. Huang, L.-E. Yang, Q.-Z. Luo, Free vibration of axially functionally graded Timoshenko beams with non-uniform cross-section, *Composites Part B: Engineering,* Vol. 45, No. 1, pp. 1493-1498, 2013.

[24] D. Jha, T. Kant, R. Singh, Higher order shear and normal deformation theory for natural frequency of functionally graded rectangular plates, *Nuclear Engineering and Design,* Vol. 250, pp. 8-13, 2012.

[25] A. Karamanlı, Analytical solutions for buckling behaviour of two directional functionally graded beams using a third order shear deformable beam theory, *Academic Platform-Journal of Engineering and Science,* Vol. 6, No. 2, pp. 164-178, 2018.

[26] M. J. Ketabdari, A. Allahverdi, S. Boreyri, M. F. Ardestani, Free vibration analysis of homogeneous and FGM skew plates resting on variable Winkler-Pasternak elastic foundation, *Mechanics & Industry,* Vol. 17, No. 1, pp. 107, 2016.

[27] M. M. Khoram, M. Hosseini, A. Hadi, M. Shishehsaz, Bending analysis of bidirectional FGM Timoshenko nanobeam subjected to mechanical and magnetic forces and resting on Winkler–Pasternak foundation, *International Journal of Applied Mechanics,* Vol. 12, No. 08, pp. 2050093, 2020.

[28] J. Kim, K. K. Żur, J. Reddy, Bending, free vibration, and buckling of modified couples stress-based functionally graded porous micro-plates, *Composite Structures,* Vol. 209, pp. 879-888, 2019.

[29] L. O. Larbi, A. Kaci, M. S. A. Houari, A. Tounsi, An efficient shear deformation beam theory based on neutral surface position for bending and free vibration of functionally graded beams#, *Mechanics Based Design of Structures and Machines,* Vol. 41, No. 4, pp. 421-433, 2013.

[30] M. Mohammadi, A. Farajpour, M. Goodarzi, H. Shehni nezhad pour, Numerical study of the effect of shear in-plane load on the vibration analysis of graphene sheet embedded in an elastic medium, *Computational Materials Science,* Vol. 82, pp. 510-520, 2014/02/01/, 2014.

[31] M. Mohammadi, A. Rastgoo, Nonlinear vibration analysis of the viscoelastic composite nanoplate with three directionally imperfect porous FG core, *Structural Engineering and Mechanics, An Int'l Journal,* Vol. 69, No. 2, pp. 131-143, 2019.

[32] M. Mohammadi, A. Rastgoo, Primary and secondary resonance analysis of FG/lipid nanoplate with considering porosity distribution based on a nonlinear elastic medium, *Mechanics of Advanced Materials and Structures,* Vol. 27, No. 20, pp. 1709-1730, 2020/10/15, 2020.

[33] M. Z. Nejad, A. Hadi, A. Rastgoo, Buckling analysis of arbitrary two-directional functionally graded Euler–Bernoulli nano-beams based on nonlocal elasticity theory, *International Journal of Engineering Science,* Vol. 103, pp. 1-10, 2016.

[34] T.-K. Nguyen, T. P. Vo, H.-T. Thai, Static and free vibration of axially loaded functionally graded beams based on the first-order shear deformation theory, *Composites Part B: Engineering,* Vol. 55, pp. 147-157, 2013.

[35] O. Rahmani, O. Pedram, Analysis and modeling the size effect on vibration of functionally graded nanobeams based on nonlocal Timoshenko beam theory, *International Journal of Engineering Science,* Vol. 77, pp. 55-70, 2014.

[36] M. Safarabadi, M. Mohammadi, A. Farajpour, M. Goodarzi, Effect of surface energy on the vibration analysis of rotating nanobeam, 2015.

[37] M. Şimşek, Fundamental frequency analysis of functionally graded beams by using different higher-order beam theories, *Nuclear Engineering and Design,* Vol. 240, No. 4, pp. 697-705, 2010.

[38] M. Şimşek, Bi-directional functionally graded materials (BDFGMs) for free and forced vibration of Timoshenko beams with various boundary conditions, *Composite Structures,* Vol. 133, pp. 968-978, 2015.

[39] M. Slimane, B. Samir, B. Hakima, H. M. Adda, Free vibration analysis of functionally graded plates FG with porosities, *International Journal of Engineering Research & Technology (IJERT),* Vol. 8, No. 03, 2019.

[40] M. Talha, B. Singh, Static response and free vibration analysis of FGM plates using higher order shear deformation theory, *Applied Mathematical Modelling*, Vol. 34, No. 12, pp. 3991-4011, 2010.

[41] H.-T. Thai, T. P. Vo, Bending and free vibration of functionally graded beams using various higher-order shear deformation beam theories, *International journal of mechanical sciences,* Vol. 62, No. 1, pp. 57-66, 2012.

[42] T. P. Vo, H.-T. Thai, T.-K. Nguyen, F. Inam, Static and vibration analysis of functionally graded beams using refined shear deformation theory, *Meccanica*, Vol. 49, No. 1, pp. 155-168, 2014.